Interdisciplinary Research in Medical Sciences Specialty
ISSN: 3062-4401
2026, Volume 6, Issue 1, Page No: 224-239

Available online at: www.galaxypub.co/page/journals

Galaxy Publication

High-Throughput Single-Cell Microarray–Based Evaluation of Immune Function in TIM3/CD28-Modified and Conventional CD19 CAR-T Cells

Daniel Kim[1]*, Jihoon Park[1], Min-seo Kang[2], Hyun-woo Jung[3]

[1]Department of CAR-T Cell Immunotherapy and Single-Cell Analysis, College of Medicine, Kyung Hee University, Seoul, South Korea.
[2]Department of High-Throughput Microarray Technology, College of Medicine, Chung-Ang University, Seoul, South Korea.
[3]Department of TIM3/CD28 Modification and Immune Function, College of Medicine, Kangwon National University, Chuncheon, South Korea.

***E-mail** ✉ jaesung.kim@khu.ac.kr

Received: 05 March 2026; **Revised:** 19 May 2026; **Accepted:** 23 May 2026

ABSTRACT

Chimeric antigen receptor (CAR) T-cell therapy has become a key treatment for blood cancers thanks to its strong capacity to identify and destroy malignant cells. Evaluating the performance of these immune cells at the individual level is essential for optimizing diagnostic and therapeutic outcomes. There is a pressing need for a versatile, rapid, high-throughput, and comprehensive system to assess immune cell efficacy. In this work, the killing ability, expansion capacity, and long-term survival of TIM3/CD28-engineered CD19 CAR-T cells were compared against standard CD19 CAR-T cells using advanced, high-throughput graphene oxide quantum dot (GOQD)-based single-cell microfluidic devices. Comprehensive profiles of secreted factors, therapeutic performance across varying effector-to-target ratios, spatial distribution effects on immune activity, and cellular subpopulation characterization were analyzed to clarify the enhanced immunotherapy potential of the modified cells. TIM3/CD28-modified CD19 CAR-T cells demonstrated superior tumor-killing activity and sustained strong therapeutic responses even under low effector-to-target ratios and at greater distances. The TIM3/CD28 modification also improved localized targeting precision. Notably, these engineered cells displayed more pronounced and stable Th1/Th2-like persistent and highly cytotoxic subpopulations, supporting more tailored therapeutic strategies. In summary, this approach offers a broadly applicable method for assessing existing CAR-T designs and testing novel CAR-based treatments moving forward.

Keywords: CAR-T, Immunotherapy effect evaluation, Microfluidic chips, Secreted factors, Single cell

How to Cite This Article: Kim D, Park J, Kang MS, Jung HW. High-Throughput Single-Cell Microarray–Based Evaluation of Immune Function in TIM3/CD28-Modified and Conventional CD19 CAR-T Cells. Interdiscip Res Med Sci Spec. 2026;6(1):224-39. https://doi.org/10.51847/SlIIhVVjvI

Introduction

The remarkable clinical success of CAR-T cell therapy against advanced hematologic malignancies has transformed cancer care by providing curative possibilities for patients with relapsed or refractory disease [1, 2]. Precise single-cell functional assessment plays a critical role in ensuring treatment accuracy and effectiveness. While CD19-targeted CAR-T cells have been thoroughly investigated [2-5], treatment failure or disease recurrence can still occur in some patients, often accompanied by off-target toxicities [3, 4]. These limitations stem from insufficient long-term persistence of the CAR-T cells [6], tumor cell resistance [2, 7], and treatment-related complications such as cytokine release syndrome (CRS) and neurotoxicity [8, 9].

Incorporation of costimulatory domains has shown that 4-1BB-containing CARs tend to promote greater durability compared with CD28-containing designs [4, 10], whereas CD28 domains drive stronger immediate effector responses [11, 12]. Advances in genetic engineering have enabled the development of multi-antigen

recognition strategies, such as dual-targeting CD19-CD22, CD19-CD20, or CD19-CD123 CARs, to overcome antigen-loss relapse [13-15]. However, balanced reactivity against each antigen remains crucial, as preferential targeting of one antigen does not fully resolve recurrence driven by antigen-negative variants [16].

Combining CAR-T therapy with immune checkpoint blockade offers synergistic benefits for enhancing anti-tumor potency and longevity—for instance, integrating costimulatory signals with PD-1 inhibition [17]. TIM3 ligands are widely present on lymphoma cell surfaces [18-20], and incorporating TIM3/CD28 reversal receptors can redirect inhibitory signals into stimulatory ones, thereby reducing immune evasion and boosting CAR-T effectiveness.

Validating these approaches, refining CAR-T performance, and enabling personalized regimens require robust functional and safety evaluation of CAR-T products. Yet, the high response rates and limited non-responder populations in leukemia patients complicate the establishment of comprehensive response parameters [21]. While many studies have examined CAR-T cells through genetic profiling [22, 23], secreted proteins provide more immediate, rapid, and reliable indicators of function, given the variability inherent in gene expression and protein synthesis. Bulk supernatant analyses have been common [18], but they overlook substantial cellular heterogeneity and lose valuable single-cell insights [24].

Furthermore, the extended in vitro manufacturing period for CAR-T cells can be life-threatening for some patients who deteriorate before infusion [3, 4]. Evidence indicates that effective doses can be quite low, though optimal dosing varies by patient condition [25]. Post-infusion expansion is important [3, 26], yet at initial infusion CAR-T cells are vastly outnumbered by target cells [4]. This leads to distinct in vivo interaction patterns—distant non-contact and close-contact modes—that produce different secretory profiles (termed spatial effects). These spatial dynamics have not been adequately studied in existing models. Patient-specific evaluation, multi-cytokine-based T-cell subset classification, and identification of optimal CAR-T characteristics for different individuals are also needed [27].

To address these gaps, TIM3/CD28-modified CD19 CAR-T cells were generated by introducing TIM3/CD28 reversal receptors onto the CD19 CAR backbone, converting inhibitory TIM3 signals from lymphoma cells into CD28-mediated co-stimulation [18]. These modified cells exhibit enhanced immune functionality through reversal of inhibition into activation. To rigorously characterize their performance, we developed a precise single-cell functional evaluation platform. Using 15-plex secreted factor profiling on GOQD-based microfluidic chips, we assessed overall secretion patterns, efficacy at different effector-to-target ratios, and spatial immune effects for both TIM3/CD28-modified and standard CD19 CAR-T cells against lymphoma targets. For the first time, up to 15 secretory differences under varied contact modes (spatial effects) were efficiently measured in vitro. Results revealed that TIM3/CD28-modified CD19 CAR-T cells preserve Th1- and Th2-like responses while gaining improved persistence, proliferative capacity, and cytotoxicity. Notably, they maintained effectiveness at lower concentrations and greater distances. Clinically, this could reduce required CAR-T cell doses, shorten manufacturing timelines, lower costs, and decrease toxicity risks.

Subsequent subpopulation profiling distinguished Th1-dominant, Th2-dominant, sustained killer, transient killer, and hyper-secretory groups, enabling better matching of CAR-T products to patient needs. Crucially, the platform is extensible to functional testing of diverse CAR constructs, offering a valuable framework for future innovative CAR development.

Materials and Methods

Microfluidic chip design and fabrication

Two distinct microfluidic chip designs were developed for cell printing and antibody barcode deposition. Prior to fabrication, the intended patterns were converted into masks and patterned onto silicon wafers via photolithography. Identical photolithography and etching conditions were applied to create the silicon masters for both chips. A positive photoresist (AZ6130) was spin-coated onto a clean silicon wafer to achieve a 2 μm layer thickness. Following pre-baking, the wafers were aligned with the respective chrome masks and exposed to UV light. After development and post-exposure baking, the patterned silicon wafers underwent dry etching to form microchambers and microchannels with a depth of 24 μm. The residual photoresist was subsequently stripped from the patterned silicon masters to enable repeated use in PDMS chip production.

Cell culture

Raji and Namalwa cells were maintained in RPMI 1640 medium containing 10% fetal bovine serum. Unmodified T cells, CD19 CAR-T cells, and TIM3/CD28-modified CD19 CAR-T cells were cultured in TexMACS GMP medium supplemented with 10% fetal bovine serum and 50 IU/mL IL-2. All cultures were incubated at 37°C in a 5% CO_2 atmosphere. All CAR-T cells used in the experiments were derived from the same donor T cell source.

Construction of the chain

The CD19 CAR construct comprised a single-chain variable fragment specific for CD19, an IgG4 Fc spacer, a CD8 transmembrane domain, a 4-1BB endodomain, and the CD3ζ signaling chain of the T cell receptor. These elements were cloned into the pCDH-CMV-MCS-EF1-CopGFP lentiviral backbone (RRID: Addgene_99730) to produce the 19BBZ vector, with the resulting cells designated as CD19 CAR-T. A second lentiviral construct was created encoding the same 19BBZ CAR along with a TIM3/CD28 chimeric switch receptor fusion protein. A T2A ribosomal skipping sequence was inserted between the CAR and the TIM3/CD28 fusion to generate the modified vector, and the transduced cells were termed TIM3/CD28-modified CD19 CAR-T.

GOQD self-assembly modification

The PDMS microchamber chip and the antibody-coated glass slide underwent oxygen plasma treatment for 5 minutes. They were then submerged in 3-aminopropyl trimethoxysilane (APTES, Sigma–Aldrich) solution for 45 minutes, followed by immersion in a GOQD suspension for 45 minutes after sonication. Finally, the surfaces were cleaned again using ultrasonication.

Antibody barcode microprinting

The PDMS microfluidic chip, featuring parallel microchannels for antibody barcode deposition, was reversibly bonded to the GOQD-functionalized glass substrates. Individual capture antibodies (2 μL per channel) were introduced into the microchannel inlets. A vacuum pump was applied at the opposite outlet to draw the antibodies through, enabling precise microprinting. After printing, the PDMS layer was detached from the glass slide, yielding the completed factor-detection chip. Prior to experiments, the chip was blocked with 3% BSA to minimize non-specific binding of secreted factors. All antibodies employed in this work were anti-human antibodies.

Hybrid single-cell printing

CAR-T effector cells were first centrifuged at 1000 rpm for 4 minutes, then combined with target cells at a 1:1 ratio. The mixture was incubated for 4 hours and resuspended in 50 μL of medium at a density of 10^6 cells/mL. This cell suspension was printed onto the GOQD-modified microchamber array chip using an S-shaped printing path, sequentially covering each column of the array. Immediately afterward, the factor-detection chip was placed onto the microchamber chip, taking care to prevent bubble formation during alignment. The assembled chips were secured with a clamp and incubated in a cell culture incubator for 1 hour. This allowed CAR-T cells (labeled with carboxyfluorescein succinimidyl ester dye) and target cells (labeled with deep red cell proliferation dye) to settle and interact naturally within each microchamber. Fluorescence microscopy was then used to image and record the positions and counts of CAR-T and target cells in every microchamber. The assembly was subsequently returned to the incubator for further culture.

Secreted immune factor detection

Following 16 hours of incubation, the chip assembly was removed from the incubator. The factor-detection chip was carefully separated in 3% BSA solution and rinsed with 1% BSA. A cocktail of biotinylated detection antibodies (0.25 μg/mL for each antibody) was applied to the factor-detection chip and incubated for 45 minutes. The chip was then washed with 1% BSA solution. Next, 300 μL of 1:100 diluted APC-conjugated streptavidin was added and incubated for 30 minutes. Finally, the chip underwent thorough washing with PBS and water.

Data and statistical analysis

Fluorescence signals from the detection factors were acquired using the 635 nm laser channel on a GenePix 4400A Scanner. Cell images were captured via the brightfield, 532 nm, and 635 nm channels on a Nikon fluorescence microscope to identify cell locations and quantities. Image analysis was performed with GenePix Pro (RRID:SCR_010969) and Nikon (RRID:SCR_021068) software. The microcavity array images were first aligned,

after which the fluorescence intensity values for each band in every microchamber were extracted. Factor concentrations were determined quantitatively using the linear standard curve relationship.

Raw fluorescence data for each secreted factor were averaged, background-subtracted, converted to concentrations via the quantitative formula, and log-transformed for downstream analysis. Background signals were computed as the average fluorescence intensity from blank microchambers (N > 50). In total, 5268 CAR-T-containing microchambers were analyzed (NTIM3/CD28-modified CD19 CAR-T = 2856; NCD19 CAR-T = 2412). Background correction, statistical calculations, and subpopulation grouping of CAR-T cells were conducted using Excel (RRID:SCR_017294) and Python (RRID:SCR_008394). Figures were produced with Origin (RRID:SCR_014212), with complete statistical details included in the figure legends.

Results and Discussion

High-throughput multi-performance systematic evaluation platform for CD19 CAR-T and TIM3/CD28-modified CD19 CAR-T immune single cells

Comprehensive single-cell assessment of CAR-T function necessitates analysis of secretion profiles under varying effector-to-target ratios and spatial conditions, followed by subpopulation classification to guide personalized therapy. Our platform integrates a GOQD-based single-cell microarray chip with a multi-factor detection chip. It enables systematic evaluation of CAR-T immune functions through overall secreted factor analysis, ratio-dependent effects, spatial interaction impacts, and subset profiling. High-density GOQD bio-affinity microchambers isolate cells from external interference while preserving viability [28]. The single-cell array is paired with the barcode detection chip such that each microchamber aligns with a complete antibody barcode array, allowing specific capture of secreted factors.

Traditional PLL-coated glass substrates often struggle with uniformity, long-term stability, and detection linearity [29]. In contrast, GOQD-modified substrates provide superior consistency, stability, and low background noise; this is their first application to CAR-T single-cell evaluation.

Prior to assembly, viable CAR-T cells and target cells are mixed at defined ratios. A hybrid single-cell printing approach then creates high-density mixed arrays with varied effector-target compositions according to Poisson statistics **(Figure 1a)**. Upon pairing and sealing the chips, cells can migrate freely within their isolated microchambers, naturally generating diverse effector-target ratios and spatial configurations.

The multiplexed barcode array for CAR-T evaluation **(Figure 1b)** is organized into six functional categories covering key immune activities: cytotoxicity [30], effector functions [31], regulation [32, 33], chemotaxis [34], stimulation [35], and inflammation [36, 37]. These barcodes are microprinted using a dedicated secreted factor detection chip. Cytotoxic markers (e.g., GZMB and Perforin) directly mediate tumor cell destruction. Effector molecules (IFN-γ, TNF-α, IL-2) drive Th1-type responses. Regulatory factors, particularly IL-4, promote Th2 activity and can modulate anti-tumor immunity. Chemokines (MCP-1, MIP-1α) control immune cell trafficking. Stimulatory factors indicate activation levels, where excessive signaling may contribute to CRS. Inflammatory mediators trigger broader inflammatory and autoimmune cascades.

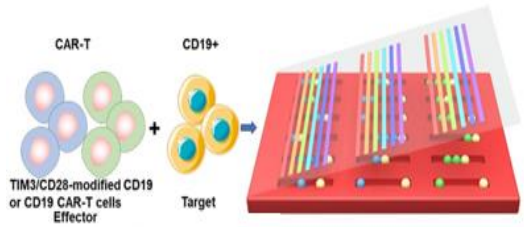

a)

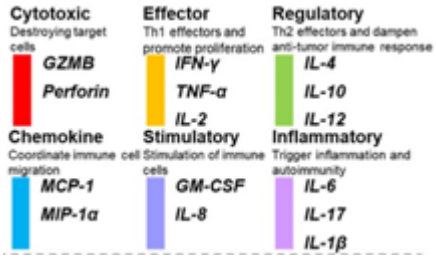

b)

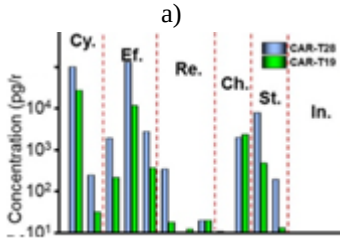

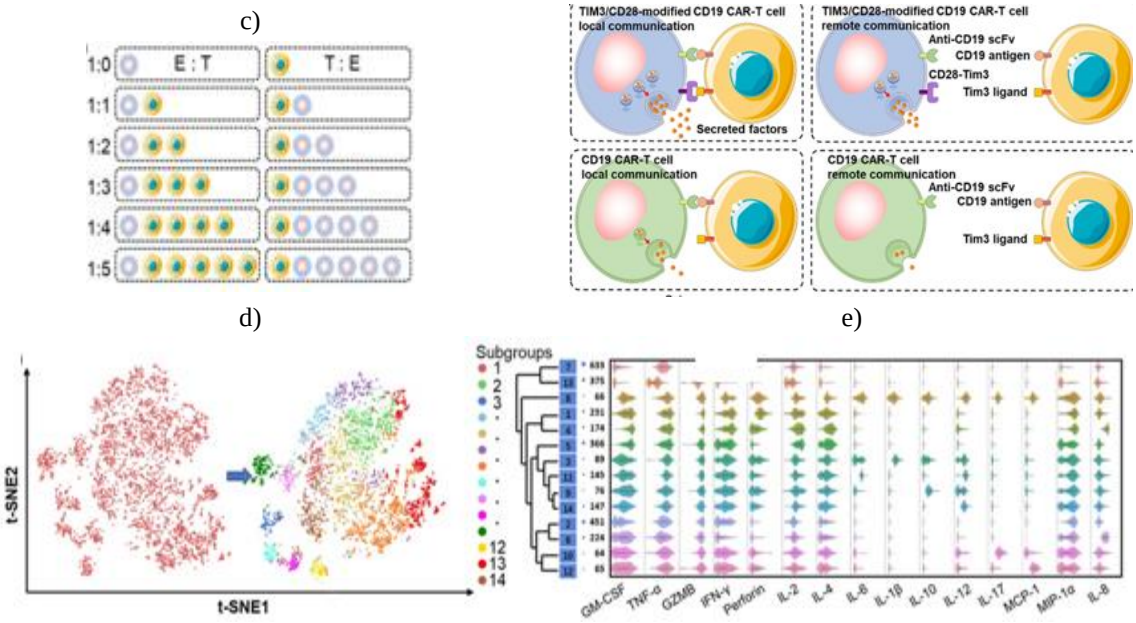

Figure 1. Schematic illustration of a high-throughput single-cell chip platform designed for comprehensive and precise functional assessment of CAR-T cells.
(a) Secreted factors released by CAR-T cells upon interaction with target cells within the cell array chip, captured and detected via an antibody barcode chip. (b) The 15-plex barcoded antibody array covering key cytokine categories: cytotoxic, effector, regulatory, chemokine, stimulatory, and inflammatory. (c) Comprehensive functional profiling of TIM3/CD28-modified CD19 CAR-T cells versus standard CD19 CAR-T cells, with the six immune function domains separated by red dashed lines. (d) Microchamber-based screening across varying effector-to-target and target-to-effector ratios. (e) Spatial analysis of functional performance for TIM3/CD28-modified CD19 CAR-T and CD19 CAR-T cells, highlighting their distinctive receptor patterns. (f) Subpopulation profiling of CAR-T cells.

The performance of the newly engineered TIM3/CD28-modified CD19 CAR-T cells was primarily assessed relative to conventional CD19 CAR-T cells. These modified cells incorporate TIM3/CD28 reversal receptors onto the CD19 CAR-T backbone, enabling the conversion of TIM3-mediated inhibitory signals into CD28-driven stimulatory signals. For a thorough functional evaluation, quantitative formulas were initially applied to compare the six core immune functions of both CAR-T variants when exposed to identical target cells **(Figure 1c)**. In contrast to conventional ELISA and flow cytometry techniques, this platform achieves greater detection throughput through multiplexed channels that avoid spectral overlap, along with enhanced sensitivity stemming from the elevated antibody density and reduced background noise provided by GOQDs. Given the variable CAR-T to target cell ratios observed across patients, the platform further examined CAR-T efficacy under different effector-target ratios in a simulated microenvironment **(Figure 1d)**. Moreover, accounting for the intricate spatial arrangements between effector and target cells in physiological settings, the study conducted detailed assessments of CAR-T functionality at varying local and distal distances **(Figure 1e)**. Crucially, immune profiles of distinct potential subpopulations were characterized through multi-condition screening and expression analysis of CAR-T cells **(Figure 1f)**. This approach uncovered numerous spatial and subpopulation features undetectable by traditional gene expression, bulk culture supernatant, or serum-based analyses [23, 38, 39]. The technique is rapid, holistic, and highly accurate, offering unique advantages and supporting tailored therapeutic strategies. In vivo mouse tumor treatment experiments with CAR-T cells were performed in prior research [18]. The current study focuses on in vitro evaluation of the secretory microenvironment between CAR-T and target cells using a single-cell platform.

Comprehensive secretory factor profiling of single CD19 CAR-T and TIM3/CD28-modified CD19 CAR-T cells
To compare the overall functional capacity of the two CAR-T types, TIM3/CD28-modified CD19 CAR-T and standard CD19 CAR-T cells were co-printed with Namalwa target cells at equal ratios. Secretion data were then collected from individual CAR-T and target cell microchambers across the entire array. The secretion factor

heatmap for TIM3/CD28-modified CD19 CAR-T cells interacting with Namalwa tumor cells is presented in **Figure 2a**, with the matching cell distribution map in **Figure 2b**. Additionally, TIM3/CD28-modified CD19 CAR-T cells were tested against Raji tumor cells to examine their activity toward alternative targets. Unmodified T cells served as negative controls. The six major immune functions (cytotoxic, effector, regulatory, chemokine, stimulatory, and inflammatory) were quantified using calibrated formulas based on fluorescence intensities from 15 recombinant factors across a 10-fold concentration series. Relative to standard CD19 CAR-T cells, the TIM3/CD28 switch receptor-engineered cells exhibited elevated secretion of Granzyme B (GZMB), IFN-γ, TNF-α, IL-2, IL-4, GM-CSF, IL-8, and others **(Figure 2c)**. To investigate responses against different targets, expression profiles of TIM3/CD28-modified CD19 CAR-T cells directed at Namalwa versus Raji tumor cells were also compared. Cytotoxic, effector, regulatory, and inflammatory factor levels were largely comparable, whereas chemokine expression increased and stimulatory factor expression decreased when targeting Raji cells. Notably, GZMB, a potent cytotoxic mediator, underscores the enhanced direct tumor-killing potential of TIM3/CD28-modified CD19 CAR-T cells. TNF-α contributes to sustained killing effects [40, 41], while IL-2 serves as a critical proliferation driver [31, 42]. The modified cells displayed 3–4-fold higher TNF-α and IL-2 levels than standard CD19 CAR-T cells **(Figure 2d)**, analyzed across four quadrants. The upper-right quadrant revealed that TNF-α+ IL-2+ double-positive cells comprised 85.4%, indicating superior proliferative capacity and prolonged tumor-killing activity in the TIM3/CD28-modified CD19 CAR-T population.

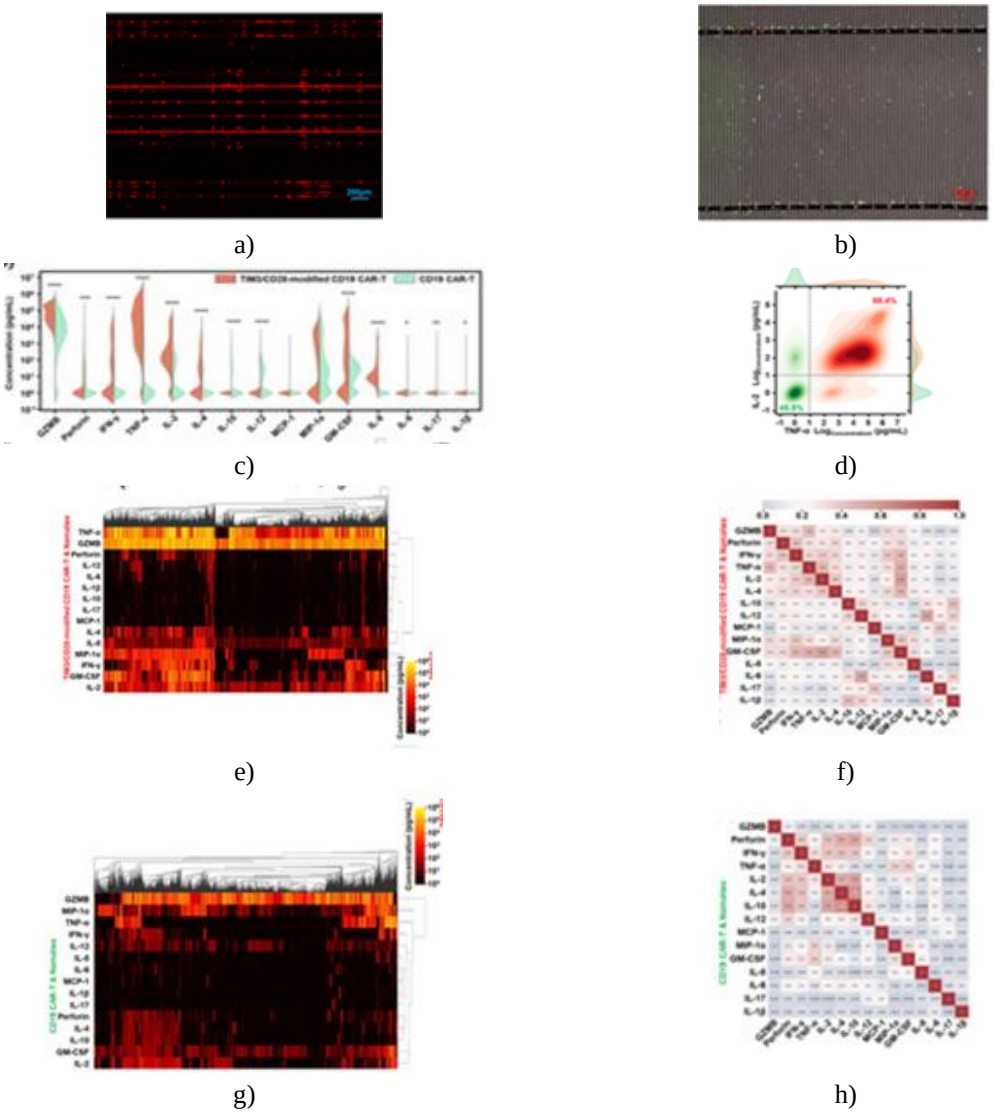

Figure 2. Superior antitumor activity of TIM3/CD28-modified CD19 CAR-T cells demonstrated through global immune function assessment.

(a) Heatmap depicting secreted factors from TIM3/CD28-modified CD19 CAR-T cells interacting with Namalwa tumor cells. (b) Fluorescence image showing TIM3/CD28-modified CD19 CAR-T cells and

Namalwa cells within microchambers, where effector cells appear green and target cells appear red. (c) Quantitative comparison of immune factor levels between TIM3/CD28-modified CD19 CAR-T and standard CD19 CAR-T cells. *$p < 0.05$, **$p < 0.01$, ***$p < 0.001$, ****$p < 0.0001$; Mann-Whitney U test. (d) Kernel density plots for the proliferation cytokine IL-2 and the sustained-killing cytokine TNF-α in both CAR-T populations, with red indicating TIM3/CD28-modified CD19 CAR-T and green indicating CD19 CAR-T. (e) Secretion heatmap for TIM3/CD28-modified CD19 CAR-T cells. (f) Correlation matrix of secreted factors from TIM3/CD28-modified CD19 CAR-T cells. (g) Secretion heatmap for CD19 CAR-T cells. (h) Correlation matrix of secreted factors from CD19 CAR-T cells.

TIM3/CD28-modified CD19 CAR-T cells displayed robust engagement in Th1-type immune responses, generating elevated levels of Th1-associated effector molecules such as IFN-γ, TNF-α, and IL-2 [43, 44]. Given that TIM3 functions as a negative regulator of antitumor immunity and is upregulated in activated CD4+ Th1-like CAR-T cells [45], the incorporation of TIM3/CD28 reversal receptors likely promotes enhanced Th1 effector production in these cells. Research indicates that balanced Th1/Th2 functionality is essential for achieving durable clinical remissions in patients [22]. Consequently, the combined secretion of Th1 effectors may serve as a marker for prolonged CAR-T cell persistence. The modified cells also showed strong activity in Th2-like processes, with increased production of Th2-related drivers and the effector IL-4, which further supports their longevity. As a co-stimulatory signal, CD28 contributes to chemokine generation [46, 47], and elevated MIP-1α expression was observed in the CART-28 variant compared with standard CD19 CAR-T. Upon activation, TIM3/CD28-modified CD19 CAR-T cells upregulated potentially hazardous cytokines including GM-CSF and IL-8. While IL-6 and MCP-1 were not detected under in vitro conditions, such factors could contribute to side effects like cytokine release syndrome (CRS) and neurotoxicity in vivo. Although overall levels of additional cytokines such as IL-10, MCP-1, IL-6, IL-17, and IL-1β remained modest, the heatmaps **(Figures 2e and 2g)** revealed the presence of highly secreting subpopulations in both TIM3/CD28-modified CD19 CAR-T and standard CD19 CAR-T groups. Following co-culture and heatmap clustering, the populations segregated primarily into high-multi-cytokine secreting TIM3/CD28-modified CD19 CAR-T cells and low-secreting CD19 CAR-T cells. Likewise, when combining data from TIM3/CD28-modified CD19 CAR-T cells targeting Namalwa and Raji cells, heatmap analysis identified two distinct clusters driven by key secreted molecules such as MCP-1. These cytokines exhibited intricate interrelationships **(Figures 2f and 2h)**. In TIM3/CD28-modified CD19 CAR-T cells, strong correlations existed among IFN-γ, TNF-α, IL-2, IL-4, and GM-CSF, particularly among Th1 effectors. In standard CD19 CAR-T cells, notable correlations were observed between perforin, IL-2, IL-4, and IL-10, suggesting potential synergistic interactions.

The underlying mechanisms of these complex correlations warrant further investigation from multiple angles. In summary, relative to standard CD19 CAR-T cells, the TIM3/CD28 modification enables higher secretion of GZMB, IFN-γ, TNF-α, IL-2, IL-4, and related factors in the engineered cells. This results in amplified cytotoxicity, enhanced proliferative potential, and extended responsiveness to antigen stimulation, culminating in improved overall antitumor efficacy. Nevertheless, the same TIM3/CD28-modified CD19 CAR-T cells also produced greater amounts of potentially risky stimulatory cytokines such as GM-CSF and IL-8 compared with standard CD19 CAR-T cells, which could trigger adverse events including CRS and neurotoxicity upon in vivo administration.

Assessment of therapeutic efficacy under varying effector-to-target ratios for single CD19 CAR-T and TIM3/CD28-modified CD19 CAR-T cells

Analysis of CAR-T cell performance across different effector-to-target (E:T) ratios holds critical importance, as immunotherapy involves dynamic phases of proliferation and apoptosis [48, 49] that generate heterogeneous E:T microenvironments in vivo. Precise pre-infusion evaluation of optimal dosing in vitro is necessary to maximize therapeutic outcomes for diverse CAR-T products, reduce production timelines, and enable individualized care. Additional screening of microchambers containing varied E:T ratios was conducted to rigorously assess cellular functions **(Figure 3a)**. Optimized hybrid single-cell printing was achieved using a 1:1 mixture of red- and green-labeled cells, facilitating the generation of thousands of 1:1 effector-target microchambers. Following equal-ratio mixing and compartmentalization, the two CAR-T variants displayed distinct proportions of multi-effector (>2:1) and multi-target (>2:1) microchambers **(Figure 3b)**. Compared with TIM3/CD28-modified CD19 CAR-T cells, the proportion of multi-effector microchambers (high CAR-T density) in standard CD19 CAR-T decreased by

4%, while the proportion of multi-target microchambers (low CAR-T density) increased by 5%. This shift arises from differential tumor-killing potency during the pre-mixing activation phase. The stronger tumoricidal activity of TIM3/CD28-modified CD19 CAR-T cells leads to higher multi-effector ratios and lower multi-target ratios. The modest magnitude of change is attributable to the 4-hour pre-mixing period prior to single-cell printing onto the chips. Cytotoxicity was subsequently compared by measuring GZMB concentrations after 16 hours at various E:T ratios for both CAR-T types against Namalwa cells. Results confirmed that TIM3/CD28-modified CD19 CAR-T cells possessed superior tumor-killing capacity over standard CD19 CAR-T cells. These single-cell findings align closely with bulk population cytotoxicity data obtained via LDH assays at different E:T ratios in earlier studies [18].

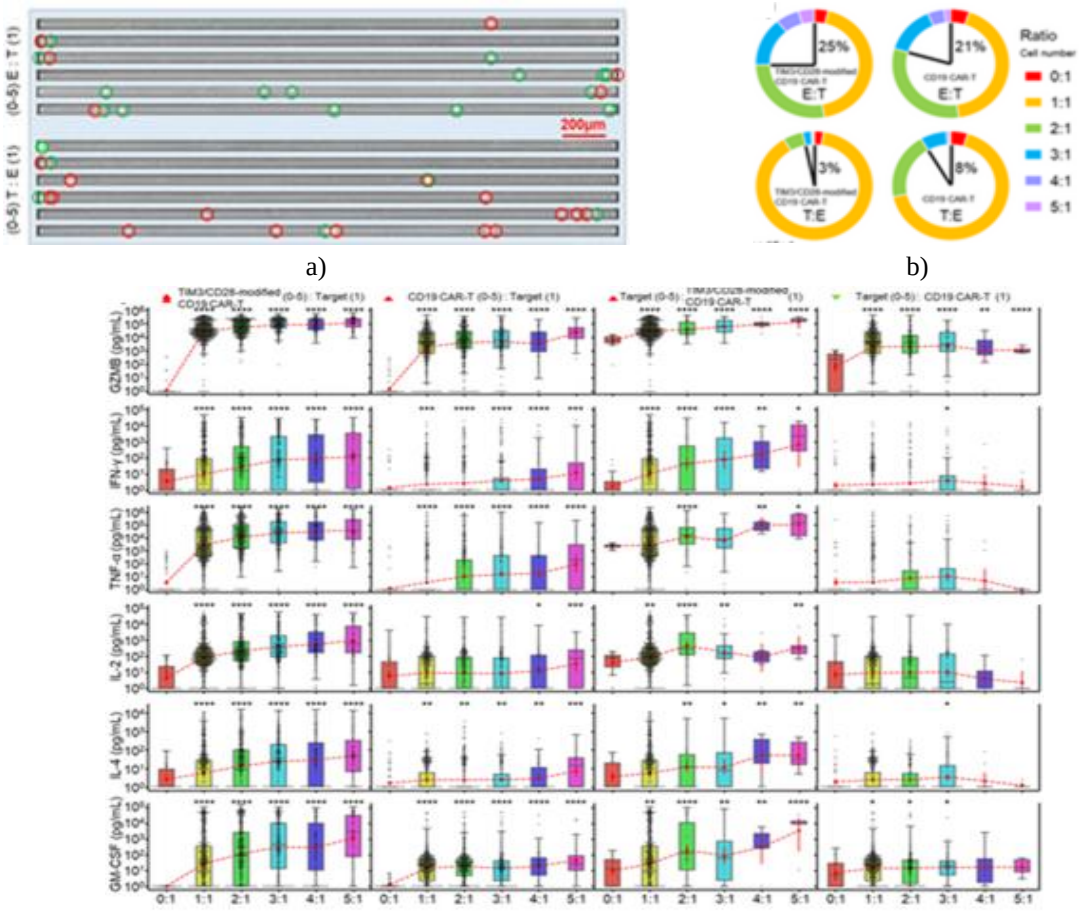

Figure 3. TIM3/CD28 reversal receptors allow TIM3/CD28-modified CD19 CAR-T cells to sustain robust therapeutic performance across both low and high effector-to-target ratios.
(a) Representative images of microchambers containing varying effector-to-target ratios; target cells are labeled red and effector cells are labeled green. (b) Distribution of microchambers for the two CAR-T variants across different effector-to-target ratios (central values in circles indicate the percentage of chambers where the dominant cell type exceeds the minority cell type by more than twofold). (c) Quantitative trends in secretion of key immune factors (GZMB, IFN-γ, TNF-α, IL-2, IL-4, and GM-CSF) within microchambers of TIM3/CD28-modified CD19 CAR-T and standard CD19 CAR-T cells at different effector-to-target ratios. Data are shown as individual values (scatter points), median (horizontal line), interquartile range (box), and mean (red dot), with trends linked by red dashed lines. Statistical comparisons for every effector-target ratio condition were made against chambers containing only target or only effector cells (0:1). *p < 0.05, **p < 0.01, ***p < 0.001, ****p < 0.0001; two-tailed Student's t test.

To elucidate the mechanisms underlying these observations, secretion levels of several critical cytokines (GZMB, IFN-γ, TNF-α, IL-2, IL-4, and GM-CSF) were quantitatively examined across the range of effector-to-target ratios for both cell types **(Figure 3c)**. In chambers containing solely target cells (E:T = 0:1), virtually no effector

molecules were measurable. As the number of CAR-T cells progressively rose from 1 to 5 while paired with single target cells, immune factor secretion increased correspondingly. For TIM3/CD28-modified CD19 CAR-T cells, GZMB secretion rose in proportion to cell number, but IFN-γ, TNF-α, IL-2, IL-4, and GM-CSF showed disproportionately larger increases (10–100-fold) relative to the modest 5-fold rise in cell count. In contrast, standard CD19 CAR-T cells performed less effectively, with factor increases generally below 10-fold. Certain cytokines, such as IFN-γ and IL-2, exhibited minimal or flat responses that lagged behind the cell number increase; at the 1:1 ratio, their concentrations were 1–2 times lower than those observed in TIM3/CD28-modified cells. These patterns demonstrate that TIM3/CD28-modified CD19 CAR-T cells possess superior proliferative and cytotoxic capabilities compared with standard CD19 CAR-T cells under both balanced (1:1) and high effector (>1:1) concentrations. Furthermore, in chambers with only effector cells (T:E = 0:1), limited effector molecules were detected due to prior activation during the 4-hour pre-mixing step. Standard CD19 CAR-T cells displayed a declining secretion trend as target cell numbers increased from 1 to 5 with single effector cells. Encouragingly, TIM3/CD28-modified CD19 CAR-T cells maintained relatively stable output for most factors except IL-2; the remaining five cytokines exhibited exponential rises that even exceeded the multi-effector secretion levels of standard CD19 CAR-T cells. Consequently, even at low concentrations (<1:1) that may occur in vivo, TIM3/CD28-modified CD19 CAR-T cells retain strong proliferative and tumor-killing capacities. This enables effective therapeutic activity even with minimal in vitro expansion. The fundamental cause lies in the TIM3/CD28 receptors' ability to convert inhibitory signals into activating ones. Standard CD19 CAR-T cells receive inhibitory inputs from TIM3 ligands, whereas the modified version receives stimulatory signals from the same ligands. This fundamental divergence leads to higher proportions of multi-effector microchambers and reduced multi-target microchambers for the TIM3/CD28-modified variant.

TIM3/CD28-modified CD19 CAR-T cells achieve superior therapeutic outcomes compared with standard CD19 CAR-T cells at very low cell densities and display consistent proliferative capacity as their numbers increase. Once effector numbers surpass target cells, the modified cells can drive exponential gains in efficacy. By comparison, standard CD19 CAR-T cells require expansion to at least a 1:1 effector-to-target ratio or higher to enhance performance, yet their functional gains remain sub-proportional to the quantitative increase. In summary, TIM3/CD28-engineered CD19 CAR-T cells demonstrate outstanding cytotoxicity at both low and high densities. This enables them to preserve effective immune activity throughout all phases—from initial infusion to treatment completion—thereby enhancing the durability of CAR-T immunotherapy.

Assessment of spatial influences on therapeutic efficacy for single CD19 CAR-T and TIM3/CD28-modified CD19 CAR-T cells

Evaluating CAR-T cell function under spatial constraints is equally critical, since CAR molecules must physically engage ligands on target cells to trigger immune activation. However, the in vivo microenvironment is highly dynamic and heterogeneous, with limited initial CAR-T cell numbers after infusion. This frequently leads to remote spatial interactions that have not been adequately characterized. Although individual TIM3/CD28-modified CD19 CAR-T cells demonstrate potent activity even at low densities, the role of spatial positioning in vivo requires careful examination. Because both effector and target cells are smaller than the microchamber dimensions, they can migrate freely within the sealed compartments. Following single-cell printing and a 1-hour incubation period, the relative positions of effector and target cells were documented. Real-time imaging distinguished "local" states, where effector cell receptors directly contact target cell ligands, from "remote" states, where the cells remain separated. These two spatial configurations were screened and analyzed in 1:1 effector-to-target microchambers **(Figure 4a)**. Statistical evaluation of approximately 1000 microchambers revealed differing distributions of the two spatial states between the CAR-T variants. TIM3/CD28-modified CD19 CAR-T cells exhibited 18% more local contacts than standard CD19 CAR-T cells, indicating a greater tendency for targeted interactions following TIM3/CD28 engineering **(Figure 4b)**. Quantitative radar plots of secreted factors under the two spatial conditions for both CAR-T types are shown in **Figures 4c and 4e**.

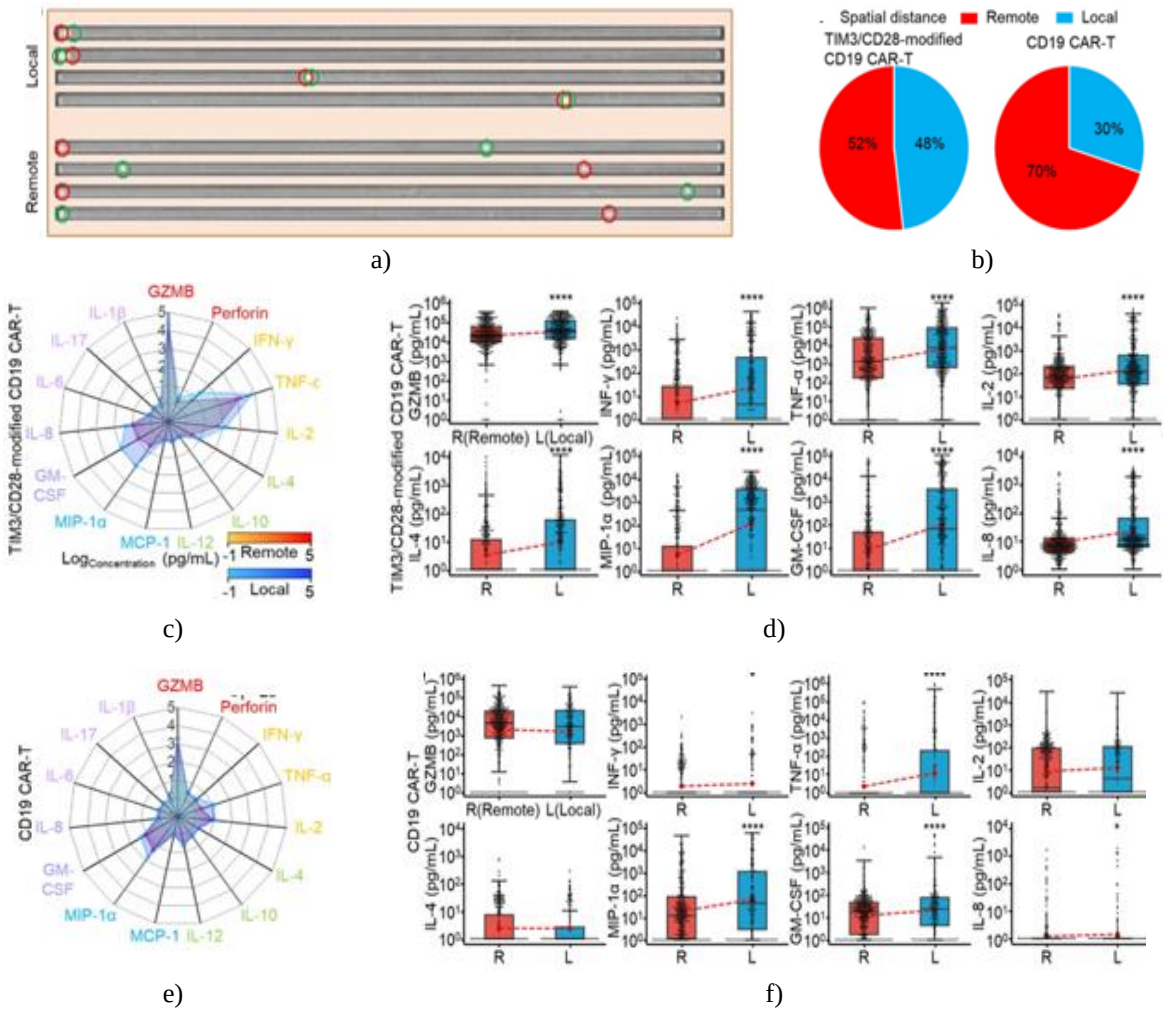

Figure 4. TIM3/CD28 reversal receptors improve local engagement and remote bystander therapeutic activity of TIM3/CD28-modified CD19 CAR-T cells.

(a) Representative images illustrating local contact and remote non-contact spatial configurations, with target cells labeled red and effector cells labeled green. (b) Distribution of 1:1 effector-to-target microchambers for the two CAR-T types under the different spatial conditions. (c) 15-plex secreted factor radar charts for TIM3/CD28-modified CD19 CAR-T cells in the two spatial states. (d) Quantitative comparison of eight immune factors showing significant differences between spatial conditions in TIM3/CD28-modified CD19 CAR-T cells. Data are displayed as individual values (scatter), median (line), quartiles (box), and mean (red dot), connected by red dashed lines. Sample sizes (N) correspond to those in (B). All statistical tests in this panel compare each spatial condition against the remote spatial condition. *$p < 0.05$, **$p < 0.01$, ***$p < 0.001$, ****$p < 0.0001$; two-tailed Student's t test. (E) 15-plex secreted factor radar charts for CD19 CAR-T cells under the two spatial states. (F) Quantitative comparison of eight immune factors showing significant differences between spatial conditions in CD19 CAR-T cells. Sample sizes (N) correspond to those in (B). All statistical tests follow the same approach as in (D).

Comparison of secretion profiles between the two CAR-T populations revealed that TIM3/CD28-modified CD19 CAR-T cells exhibit broad expansion of factor release following local contact. Most molecules—including the cytotoxic mediator GZMB, Th1 effectors IFN-γ, TNF-α and IL-2, the Th2 cytokine IL-4, the chemokine MIP-1α, and the stimulatory factors GM-CSF and IL-8—showed increases approaching or exceeding tenfold. In contrast, local contact in standard CD19 CAR-T cells produced only modest elevations in TNF-α, MIP-1α, and GM-CSF, with the overall secretion pattern remaining largely stable and certain factors such as GZMB even displaying reduced output. These results indicate that the TIM3/CD28 receptor effectively transforms inhibitory inputs into stimulatory signals, driving substantially higher release of functional cytokines upon direct contact in the modified cells and thereby conferring stronger immune activation.

Notably, TIM3/CD28-modified CD19 CAR-T cells maintained robust secretion even in the absence of direct contact. This suggests alternative activation mechanisms within the surrounding microenvironment when physical interaction with target cells is absent. Relative to standard CD19 CAR-T cells, the modified cells secreted higher amounts of the direct killer GZMB, Th1 effectors IFN-γ, TNF-α and IL-2, while producing lower levels of the stimulatory cytokine GM-CSF during remote, non-contact activation. This profile enhances killing capacity, proliferation potential, and persistence while diminishing the risk of indirect toxic side effects at distant sites that commonly arise under low cell-density conditions. Although GM-CSF and IL-8 levels decreased in remote non-contact scenarios, both activated TIM3/CD28-modified CD19 CAR-T and standard CD19 CAR-T cells still released cytokines capable of contributing to CRS and neurotoxicity. Importantly, this represents a manageable drawback of the TIM3/CD28-modified CD19 CAR-T design that does not preclude favorable clinical translation in the future.

To highlight these distinctions more precisely, eight key differentially regulated factors—GZMB, IFN-γ, TNF-α, IL-2, IL-4, MIP-1α, GM-CSF, and IL-8—were subjected to detailed statistical analysis **(Figures 4d and 4f)**. TIM3/CD28-modified CD19 CAR-T cells demonstrated enhanced therapeutic potential after local contact, whereas standard CD19 CAR-T cells (CART-19) displayed neutral or inhibitory responses characterized by unchanged or decreased secretion. Although non-contact conditions also diminished some functional outputs in the modified cells, their performance in the remote state still surpassed that of contact-activated standard CD19 CAR-T cells. These findings offer a novel framework and approach for assessing the immune functionality of CAR-T cells engineered with other innovative receptors using microfluidic platforms, with particular emphasis on spatial dynamics.

Investigation of Th1/Th2-balanced, long-persisting, and high-potency killer CAR-T subpopulations integrating effector-target ratios and spatial influences

CD19 CAR-T therapy achieves high response rates in both pediatric and adult patients with B-cell acute lymphoblastic leukemia (B-ALL). Although approximately 90% of patients reach remission, over 50% fail to sustain long-term disease control and remain at risk of relapse [50-52]. Additionally, variable CD4/CD8 ratios within CAR-T products [53, 54] contribute to heterogeneous subpopulations, complicating functional assessment and making patient-tailored manufacturing both time-intensive and costly. Therefore, robust secreted-factor-based criteria for subpopulation evaluation are urgently required to better predict treatment durability and effectiveness. While flow cytometry enables rapid phenotypic analysis, it captures only endpoint cellular properties [55] and does not reflect the dynamic responses of CAR-T cells following target cell engagement. Spectral overlap further restricts its multiplexing capacity for multifunctional profiling [56]. Prior research has linked Th1 activity to improved cell longevity, emphasized the importance of Th2 function for sustained remission, and shown that co-existence of Th1 and Th2 activities correlates with durable responses, whereas Th2 deficiency is commonly associated with CD19-positive relapse [22, 43, 57].

To identify distinctive subpopulations suitable for personalized applications, the study accounted for the multifaceted conditions present in vivo by evaluating subgroups under varying effector-target ratios and spatial configurations. A K-means t-SNE clustering approach [58] was applied to categorize CAR-T subpopulations, with the K value initially set to three times the number of highly expressed factors and iteratively reduced until no redundant clusters remained [28]. The two CAR-T types—TIM3/CD28-modified CD19 CAR-T and standard CD19 CAR-T—were collectively partitioned into 26 subpopulations based on their 15-plex secretion profiles **(Figure 5a)**. Subpopulation proportions are displayed in **Figure 5b**. Expression distributions for the six major immune function categories within each subpopulation are illustrated via violin plots in **Figure 5c**, while inter-subpopulation relationships appear in the left dendrogram of the hierarchical clustering tree. All standard CD19 CAR-T cells clustered within the weak immune function branch (green), which also included the low-expression subgroups 1, 5, and 6 from TIM3/CD28-modified CD19 CAR-T cells. Notably, no standard CD19 CAR-T subpopulations fell into the strong immune function branch (blue). Raji-targeted modified CAR-T cells resolved into 13 subpopulations, many displaying strong immune function alongside weaker clusters such as subgroup-7. Their RadViz secretion profiles are characterized by unique molecular signatures. Unmodified T cells separated into five subpopulations, with subgroup-2 comprising 89.6% of cells and showing essentially no cytokine secretion.

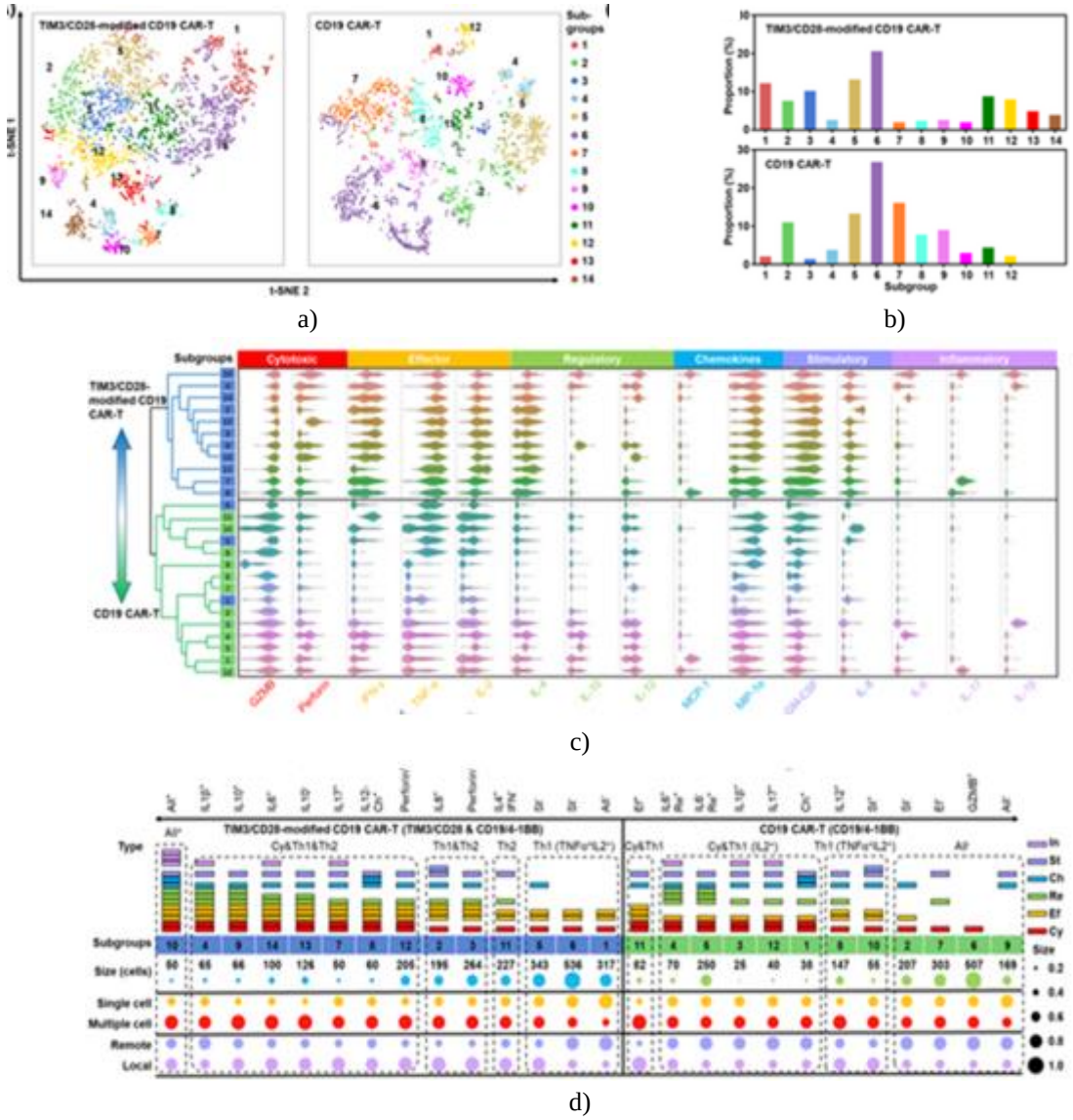

Figure 5. TIM3/CD28-modified CD19 CAR-T cells exhibited a greater presence of coexisting Th1 and Th2 long-term persistent and highly effective killer subpopulations compared to standard CD19 CAR-T cells. (a) Identified subpopulations within TIM3/CD28-modified CD19 CAR-T and CD19 CAR-T cells, with cluster sizes (N) noted as in panel (D). (b) Relative proportions of the various subpopulations in both types of CAR-T cells. (c) Violin plots displaying the immune functional profiles of subpopulations, along with hierarchical clustering for classification of TIM3/CD28-modified CD19 CAR-T (indicated in blue) and CD19 CAR-T (indicated in green). (d) Examination of positive secretory profiles in TIM3/CD28-modified CD19 CAR-T and CD19 CAR-T cells, including counts of different immune secretion categories, effector-to-target ratios, and spatial interaction patterns across all subpopulations. Visualizations in panels (A, C, D) were generated using Python.

Additionally, in-depth analysis was performed on the results for each subpopulation of the two CAR-T variants targeting the same antigen (Namalwa cells). A minimum expression threshold of 10 pg/mL was applied to classify each immune factor as positive (e.g., IL-2+) or negative (e.g., IL-2-). This threshold was used across categories of immune functions, including cytotoxic, effector, regulatory, chemokine, stimulatory, and inflammatory responses. Subpopulations of TIM3/CD28-modified CD19 CAR-T and CD19 CAR-T cells were arranged from left to right based on the total number of positively expressed immune factors **(Figure 5d)**.

Notably, the weakly functional subpopulations (1, 4, and 5) of TIM3/CD28-modified CD19 CAR-T ranked at the lower end among its own groups. In contrast, among the weakly functional CD19 CAR-T subpopulations, only two (subgroups 4 and 5) expressed more than eight immune factors, whereas nine such subgroups were observed in TIM3/CD28-modified CD19 CAR-T cells. As previously noted, Th1-type responses can substantially enhance

CAR-T cell survival and persistence, typically involving high secretion of effector molecules such as IFN-γ, TNF-α, and IL-2 [43, 44]. Every subpopulation of TIM3/CD28-modified CD19 CAR-T cells showed positive expression of at least two Th1 effectors, while only subgroup 11 (4.3%) of CD19 CAR-T cells demonstrated a robust Th1 response. Furthermore, despite the presence of several low-secretion subgroups (1, 5, and 6) in TIM3/CD28-modified CD19 CAR-T cells, these still expressed critical factors including the cytotoxic molecule GZMB and effector cytokines TNF-α and IL-2. Such expression supports strong direct and sustained killing capacity as well as proliferative potential. The lack of excessive stimulatory and inflammatory factors in these cells may also help lower the risk of cytokine release syndrome (CRS).

Th2-type responses can additionally promote CAR-T cell persistence, with IL-4 serving as a key marker [59]. Except for the weak subgroups 1, 5, and 6, nearly all TIM3/CD28-modified CD19 CAR-T subpopulations expressed IL-4, whereas only subgroups 4 and 5 in CD19 CAR-T cells did so. Moreover, TIM3/CD28-modified CD19 CAR-T cells lacked many of the severely immune-deficient subpopulations seen in CD19 CAR-T cells, where the dominant groups displayed clear functional impairment. Perforin-deficient cells were identified in both CAR-T types. Overexpression of the stimulatory pro-inflammatory factor IL-8 occurred in perforin-deficient TIM3/CD28-modified CD19 CAR-T subgroup 2 and CD19 CAR-T subgroup 10.

Statistical evaluation of the diversity of immune secretion types, along with effector-target ratios and spatial configurations across subpopulations, aligned with the patterns described. Blue-green bubbles denote the two CAR-T cell types, with bubble size reflecting subpopulation scale. Yellow-red bubbles indicate the proportions of single versus 2–5 multiple CAR-T cells engaging a single target cell. Purple-pink bubbles represent the proportions of remote versus local spatial interaction modes within each subpopulation **(Figure 5d)**. It was evident that most multi-positive immune subpopulations featured higher proportions of multi-cell engagements and local contact spatial patterns, indicating cooperative cellular effects. Th1-dominant subpopulations particularly showed elevated rates of local contact. Even in CD19 CAR-T cells, a limited number of subgroups (11, 8, and 10) displayed this trait, associated with strengthened Th1 activity. The TIM3/CD28 modification appeared to mitigate contact inhibition, increasing the proportion of local contacts in TIM3/CD28-modified CD19 CAR-T cells and thereby enhancing multi-cellular immune performance.

Overall, among TIM3/CD28-modified CD19 CAR-T cells: 2.0% belonged to the super-secreting subgroup 10; 25.8% represented direct-killing cells with coexisting Th1/Th2 responses; subgroups 4, 7, 8, 9, 12, 13, and 14 (17.6%) showed durable Th1/Th2 coexistence; subgroups 2 and 3 (8.7%) and subgroup 11 (11%) corresponded to durable Th2 responses; and 45.9% fell into weakly Th1 but lower-toxicity subgroups 1, 5, and 6. For CD19 CAR-T cells: 4.3% were in the mildly reduced killing/Th1 subgroup 11; 22.4% in subgroups 1, 3, 4, 5, and 12 with slightly reduced killing and proliferative capacity; 10.7% in weakly Th1 but lower-toxicity subgroups 8 and 10; and 62.7% in inhibited, largely ineffective subgroups 2, 6, 7, and 9.

Subpopulation analysis revealed that CART-28 cells possess a distinctive Th2 subpopulation in addition to expanded Th1 subpopulations and long-term persistent groups combining Th1 and Th2 functions. In comparison, CD19 CAR-T cells contained numerous Th2-deficient subpopulations, and their Th1 subpopulations rarely co-expressed all three major effectors at high levels. Killing potential in both CAR-T types was assessed via expression of cytotoxic factors GZMB and Perforin. Further assessment of effector-target ratios and spatial dynamics highlighted unique subpopulations, such as Th1-enriched groups that partially overcome inhibitory barriers and favor proximity to target cells. These precisely characterized subpopulations uncover a range of potential CAR-T immune subtypes, offering supporting data and diverse candidates for developing personalized CAR-T therapies with optimal characteristics. Nevertheless, the high expense of CAR-T products and requirements for individualized production mean this assessment approach has not yet achieved clinical implementation.

Conclusion

This study introduces a GOQD-enabled high-throughput single-cell microfluidic chip platform for assessing CAR-T cell immunotherapy performance. At the single-cell level, comprehensive profiling was conducted on secretory factor expression profiles, immunotherapy outcomes under varying effector-to-target ratios, spatial immunotherapy dynamics, and subpopulation diversity for both CD19 CAR-T and TIM3/CD28-modified CD19 CAR-T cells. The TIM3/CD28 modification enhanced the sustained tumor-targeting capacity of the engineered cells. In particular, single TIM3/CD28-modified CD19 CAR-T cells maintained strong therapeutic activity even

in remote, non-contact spatial configurations. Overall, TIM3/CD28-modified CD19 CAR-T cells displayed a richer array of distinct Th1/Th2 long-persistence and potent killer subpopulations relative to unmodified CD19 CAR-T cells. Importantly, this platform is suitable not only for evaluating these specific CAR-T combinations but also serves as a robust tool for functional testing of emerging CAR-based therapies moving forward.

Acknowledgments: None

Conflict of Interest: None

Financial Support: None

Ethics Statement: None

References

1. Grupp SA, Kalos M, Barrett D, Aplenc R, Porter DL, Rheingold SR, et al. Chimeric antigen receptor-modified T cells for acute lymphoid leukemia. N Engl J Med. 2013;368(16):1509-18.
2. Fry TJ, Shah NN, Orentas RJ, Stetler-Stevenson M, Yuan CM, Ramakrishna S, et al. CD22-targeted CAR T cells induce remission in B-ALL that is naive or resistant to CD19-targeted CAR immunotherapy. Nat Med. 2018;24(1):20-8.
3. Park JH, Rivière I, Gonen M, Wang X, Sénéchal B, Curran KJ, et al. Long-term follow-up of CD19 CAR therapy in acute lymphoblastic leukemia. N Engl J Med. 2018;378(5):449-59.
4. Maude SL, Laetsch TW, Buechner J, Rives S, Boyer M, Bittencourt H, et al. Tisagenlecleucel in children and young adults with B-cell lymphoblastic leukemia. N Engl J Med. 2018;378(5):439-48.
5. Smith M, Dai A, Ghilardi G, Amelsberg KV, Devlin SM, Pajarillo R, et al. Gut microbiome correlates of response and toxicity following anti-CD19 CAR T cell therapy. Nat Med. 2022;28(4):713-23.
6. Fucà G, Reppel L, Landoni E, Savoldo B, Dotti G. Enhancing chimeric antigen receptor T cell efficacy through metabolic modulation. Clin Cancer Res. 2020;26(10):2444-52.
7. Orlando EJ, Han X, Tribouley C, Wood PA, Leary RJ, Riester M, et al. Genetic mechanisms of target antigen loss in CAR19 therapy of acute lymphoblastic leukemia. Nat Med. 2018;24(10):1504-10.
8. Lee DW, Gardner R, Porter DL, Louis CU, Ahmed N, Jensen M, et al. Current concepts in the diagnosis and management of cytokine release syndrome. Blood. 2014;124(2):188-95.
9. Shi X, Wu H. CAR T cell exhaustion: mechanisms and therapeutic strategies. Eur J Immunol. 2022;20:1-15.
10. Cappell KM, Kochenderfer JN. Long-term outcomes following CAR T cell therapy: what we know so far. Nat Rev Clin Oncol. 2021;18(11):715-27.
11. Zhao Z, Condomines M, van der Stegen SJC, Perna F, Kloss CC, Gunset G, et al. Structural design of engineered costimulation determines tumor rejection kinetics and persistence of CAR T cells. Cancer Cell. 2015;28(4):415-28.
12. Textor A, Grunewald L, Anders K, Klaus A, Schwiebert S, Winkler A, et al. CAR T cells targeting the T cell receptor β constant domain for treatment of T cell malignancies. Cancers. 2021;13(5):1050.
13. Schneider D, Xiong Y, Wu D, Nölle V, Schmitz S, Haso W, et al. A tandem CD19/CD20 CAR lentiviral vector drives on-target and off-target antigen modulation in leukemia cell lines. J Immunother Cancer. 2017;5:42.
14. Qin H, Ramakrishna S, Nguyen S, Fountaine TJ, Ponduri A, Stetler-Stevenson M, et al. Preclinical development of bivalent chimeric antigen receptors targeting both CD19 and CD22. Mol Ther Oncolytics. 2018;11:127-37.
15. Ruella M, Barrett DM, Kenderian SS, Shestova O, Hofmann TJ, Perazzelli J, et al. Dual CD19 and CD123 targeting prevents antigen-loss relapses after CD19-directed immunotherapies. J Clin Investig. 2016;126(10):3814-26.
16. Shah NN, Fry TJ. Mechanisms of resistance to CAR T cell therapy. Nat Rev Clin Oncol. 2019;16(6):372-85.
17. Liu H, Lei W, Zhang C, Yang C, Wei J, Guo Q, et al. CD19-specific CAR T cells that express a PD-1/CD28 chimeric switch receptor exhibit improved antitumor efficacy. Clin Cancer Res. 2021;27(2):473-85.
18. Zhao S, Wang C, Lu P, Lou Y, Liu H, Wang T, et al. TGF-β signaling in CAR T cells enhances antitumor efficacy and reduces toxicity. J Immunother Cancer. 2021;9(5):e003176.

19. Monney L, Sabatos CA, Gaglia JL, Ryu A, Waldner H, Chernova T, et al. Th1-specific cell surface protein Tim-3 regulates macrophage activation and severity of an autoimmune disease. Nature. 2002;415(6871):536-41.
20. Nakayama M, Akiba H, Takeda K, Kojima Y, Hashiguchi M, Azuma M, et al. Tim-3 mediates phagocytosis of apoptotic cells and cross-presentation. Blood. 2009;113(16):3821-30.
21. Xu J, Melenhorst JJ, Fraietta JA. Toward precision manufacturing of CAR T cells for cancer immunotherapy. Cytotherapy. 2018;20(5):623-38.
22. Bai Z, Woodhouse S, Zhao Z, Arya R, Govek K, Kim D, et al. Single-cell antigen-specific activation profiling of T cells using a droplet microfluidics platform. Sci Adv. 2022;8(16):eabj2820.
23. Bai Z, Lundh S, Kim D, Woodhouse S, Barrett DM, Myers RM, et al. Single-cell analysis of CAR T cell exhaustion reveals distinct transcriptional states. J Immunother Cancer. 2021;9(8):e002328.
24. Labib M, Kelley SO. Single-cell analysis targeting the proteome. Nat Rev Chem. 2020;4(3):143-58.
25. Lee DW, Kochenderfer JN, Stetler-Stevenson M, Cui YK, Delbrook C, Feldman SA, et al. T cells expressing CD19 chimeric antigen receptors for acute lymphoblastic leukaemia in children and young adults: a phase 1 dose-escalation trial. Lancet. 2015;385(9967):517-28.
26. Fang Y, Yan Y, Bi S, Wang Y, Chen Y, Xu P, et al. Microfluidic-based single-cell analysis for CAR T cell therapy monitoring. Anal Chem. 2022;94(39):13205-14.
27. Rossi J, Paczkowski P, Shen YW, Morse K, Flynn B, Kaiser A, et al. Preinfusion polyfunctional anti-CD19 chimeric antigen receptor T cells are associated with clinical outcomes in NHL. Blood. 2018;132(8):804-14.
28. Wang C, Wang C, Wu Y, Gao J, Han Y, Chu Y, et al. Biomimetic nanocarriers for enhanced CAR T cell therapy in solid tumors. Adv Healthcare Mater. 2022;11(6):2102800.
29. Xue Q, Bettini E, Paczkowski P, Ng C, Kaiser A, McConnell T, et al. Single-cell multiplexed cytokine profiling of CD19 CAR-T cells reveals a diverse landscape of polyfunctional antigen-specific response. J Immunother Cancer. 2017;5:85.
30. Lemoine J, Ruella M, Houot R. Overcoming resistance to CAR T cell therapy in B-cell malignancies. Clin Cancer Res. 2021;27(23):6298-306.
31. Aspuria PJ, Vivona S, Bauer M, Semana M, Ratti N, McCauley S, et al. A novel IL-18 binding protein enhances CAR T cell antitumor activity. Sci Transl Med. 2021;13(616):eabg7565.
32. Stewart CM, Cox MJ, Sakemura RL, Ogbodo EJ, Can I, Manriquez-Roman C, et al. Inhibition of adenosine signaling enhances CAR T cell function. Blood. 2022;140(Suppl 1):4536-8.
33. Li J, Li W, Huang K, Zhang Y, Kupfer G, Zhao Q. Chimeric antigen receptor T cell (CAR-T) immunotherapy for solid tumors: lessons learned and strategies for moving forward. J Hematol Oncol. 2018;11(1):22.
34. Sterner RM, Sakemura R, Cox MJ, Yang N, Khadka RH, Forsman CL, et al. GM-CSF inhibition reduces cytokine release syndrome and neuroinflammation but enhances CAR T cell function in xenografts. Blood. 2019;133(7):697-709.
35. Sachdeva M, Aranda-Orgilles B, Duchateau P, Poirot L, Valton J. Engineering of CAR T cells to overcome immunosuppression. Cancer Immunol Res. 2020;8(3 Suppl):A60.
36. Norelli M, Camisa B, Barbiera G, Falcone L, Purevdorj A, Genua M, et al. Monocyte-derived IL-1 and IL-6 are differentially required for cytokine-release syndrome and neurotoxicity due to CAR T cells. Nat Med. 2018;24(6):739-48.
37. Shibabaw T. Inflammatory cytokines and their role in cancer immunotherapy. J Inflamm Res. 2020;13:673-88.
38. Nguyen NT, Huang K, Zeng H, Jing J, Wang R, Fang S, et al. Nano-optogenetic engineering of CAR T cells for precision immunotherapy. Nat Nanotechnol. 2021;16(12):1424-33.
39. Hu Q, Li H, Archibong E, Chen Q, Ruan H, Ahn S, et al. Engineering CAR T cells for enhanced persistence and activity using biodegradable nanoparticles. Nat Biomed Eng. 2021;5(9):1038-50.
40. Shen J, Xiao Z, Zhao Q, Li M, Wu X, Zhang L, et al. Anti-cancer therapy with CAR T cells: recent advances and future perspectives. Cell Prolif. 2018;51(3):e12441.
41. Ma C, Cheung AF, Chodon T, Koya RC, Wu Z, Ng C, et al. Multifunctional T-cell analyses to study response and progression in adoptive cell transfer immunotherapy. Cancer Discov. 2013;3(4):418-29.
42. Lynn RC, Weber EW, Sotillo E, Gennert D, Xu P, Good Z, et al. c-Jun overexpression in CAR T cells induces exhaustion resistance. Nature. 2019;576(7786):293-300.

43. Laheurte C, Dosset M, Vernerey D, Boullerot L, Gaugler B, Gravelin E, et al. Immunological biomarkers of response to immunotherapy in non-small cell lung cancer. Br J Cancer. 2019;121(5):405-14.
44. Pang N, Alimu X, Chen R, Muhashi M, Ma J, Chen G, et al. Immune checkpoint inhibitors in combination with CAR T cell therapy. FASEB J. 2021;35(6):e21556.
45. Banerjee H, Kane LP. Immune checkpoint blockade in CAR T cell therapy. F1000Res. 2018;7:316.
46. Marangoni F, Zhang R, Mani V, Thelen M, Ali Akbar NJ, Warner RD, et al. Tumor microenvironment modulates CAR T cell trafficking and function. J Immunol. 2018;200(10):3647-58.
47. Porciello N, Grazioli P, Campese AF, Kunkl M, Caristi S, Mastrogiovanni M, et al. CAR T cells require CD28 co-stimulation for optimal persistence and antitumor activity. Nat Commun. 2018;9(1):1080.
48. Tanaka A, Sakaguchi S. Regulatory T cells in cancer immunotherapy. Cell Res. 2017;27(1):109-18.
49. Olejarz W, Dominiak A, Żołnierzak A, Kubiak-Tomaszewska G, Lorenc T. Tumor-infiltrating lymphocytes in cancer immunotherapy. J Immunol Res. 2020;2020:6272498.
50. Maude SL, Frey N, Shaw PA, Aplenc R, Barrett DM, Bunin NJ, et al. Chimeric antigen receptor T cells for sustained remissions in leukemia. N Engl J Med. 2014;371(16):1507-17.
51. Pulsipher MA, Han X, Maude SL, Laetsch TW, Qayed M, Rives S, et al. Next-generation sequencing of CAR T cell products reveals clonal dynamics and determinants of response. Blood Cancer Discov. 2022;3(1):66-79.
52. Wang Z, Sargent EH, Kelley SO. Single-cell analysis of CAR T cell therapy using electrochemical methods. Anal Chem. 2021;93(4):2327-36.
53. Demaret J, Varlet P, Trauet J, Beauvais D, Grossemy A, Hégo F, et al. Monitoring CAR T cells using flow cytometry. Cytom Part B Clin Cy. 2021;100(2):218-27.
54. Golubovskaya V, Wu L. Different subsets of T cells, memory, effector functions, and CAR-T immunotherapy. Cancers. 2016;8(3):36.
55. Maryamchik E, Gallagher KME, Preffer FI, Kadauke S, Maus MV. Flow cytometry of CAR T cells: a practical guide. Cytom Part B Clin Cy. 2020;98(4):299-308.
56. Eyer K, Doineau RCL, Castrillon CE, Briseno-Roa L, Menrath V, Mottet G, et al. Single-cell deep phenotyping of IgG-secreting cells for high-resolution immune monitoring. Nat Biotechnol. 2017;35(10):977-82.
57. Xhangolli I, Dura B, Lee G, Kim D, Xiao Y, Fan R. Single-cell analysis of CAR T cells in cancer immunotherapy. Genom Proteom Bioinf. 2019;17(2):129-40.
58. Kiselev VY, Kirschner K, Schaub MT, Andrews T, Yiu A, Chandra T, et al. SC3: consensus clustering of single-cell RNA-seq data. Nat Methods. 2017;14(5):483-6.
59. Fowell DJ, Kim M. The spatiotemporal control of T cell responses in inflamed tissues. Nat Rev Immunol. 2021;21(9):582-96.